Proceedings of the 2017 IEEE
International Conference on Robotics and Biomimetics
December 5-8, 2017, Macau SAR, China

Design of a Double-Propellers Wall-Climbing Robot

Kanjanapan Sukvichai
Dept. of Electrical Engineering
Faculty of Engineering,
Kasetsart University, Thailand
fengkpsc@ku.ac.th

Pruttapon Maolanon
Dept. of Electrical Engineering
Faculty of Engineering,
Kasetsart University, Thailand
pruttapon.m@ku.th

Konlayut Songkrasin
Dept. of Electrical Engineering
Faculty of Engineering,
Kasetsart University, Thailand
konlayut.s@ku.th

***Abstract*—Wall-climbing robot is one of the most interesting robot because it can be used in several useful application such as inspection of high buildings, wall and mirror cleaning, surveillance and military operations. Propellers type wall-climbing robot is designed in this research. Behavior of this robot can be understood by observing its mathematical model. Aerodynamics of the propeller and robot dynamics model are obtained by using the momentum conservation and blade element theory and Euler-Lagrange equation and combined to reveal the robot mathematical model. The real climbing robot is manufactured by different materials and several methods in order to get very light weight robot. Robot consists of two propellers and four free wheels. Experiments are conducted in this research in order to check the robot performance. By using the actuating thrust and change of rotor system angle, the robot can climb the desired surface and have ability to move itself back to the climbing surface when the robot starts to fall out of the wall.**

Keywords—propeller; aerodynamics; robot dynamics; wall-climbing robot

I. INTRODUCTION

Robots are developed to help human to perform several different tasks in order to improve human's quality of life. Autonomous robot is a useful application for human specially for dangerous environments or difficult-to-access places. Wall-climbing robot is one of the interesting robot research topics because of its characteristic and abilities. Climbing robots must have ability to mobilize on the interested vertical surface and ability to hold itself to the surface when it is necessary. This kind of robot can be implemented for special works such as the inspection of high-rise buildings, spray painting, wall and mirror cleaning, aircraft inspection, surveillance and military operations. One of the most challenging topics in climbing robot design is how to develop an adhesion mechanism to ensure that the robot always stick to the surface without falling out. There are four popular types of the adhesion mechanisms which are magnetic adhesion mechanism for ferrous surfaces, aerodynamic attraction force generators, vacuum suction and bio-inspired climbing mechanisms or materials. Robots using permanent magnets or electromagnets were introduced by J. Grieco [1], W. Shen [2] and Howlader [3] in 1998, 2005 and 2015 respectively. These robots are simple but good enough for steel walls; however, their applications are limited due to the nature of magnets. Propellers type wall-climbing robots were developed by Nishi [4] and Disney research [5]. Aerodynamic thrust, generated from propellers, is used to make a robot stick to surfaces. The third technique for wall-climbing robots is done by using vacuum suction cups. There are several success wall-climbing robots using this technique such as robots that were developed by Panich [6] and Chen [7]. The limitation of this suction-based robot is that the suction cups are required perfect sealing suction chamber. Robot can move only in a slow speed because it requires time to produce and release vacuum. Bio-inspired climbing robot is the last type of the wall-climbing robot. This robot is used inspiration from real animal in both climbing mechanisms and materials. The most popular inspired animal is gecko. By using material similar to gecko foot, robot can maneuver on the wall without falling [8] [9]. In this research, the double-propellers type wall-climbing robot is selected, analyzed, designed, developed and tested because it can climb the wall without limitation of materials.

II. ROBOT ANALYSIS

Propellers type wall-climbing robot requires thrust that generated from propeller in the rotor system to hold and move itself on the interested climbing surface. The aerodynamics of the rotor system is considered at the beginning of this topic. Then, the dynamics of the robot is considered by using the conservation of energy theory. Finally, by combining aerodynamics and robot dynamics, the mathematic model of the wall-climbing robot is obtained.

A. Rotor Aerodynamics

Aerodynamics of the rotor is obtained by using the energy conversion in form of Bernoulli's equation. The blade and rotor are considered as the rotating disk that induces the air flow out from the rotor system in order to generate the down force. Then, the momentum conservation theory is applied to the rotor [10]. Because the robot is always stick to the climbing surface, thus, the robot is considered in a hover state. The thrust from the disk is equal to (1).

$$T_h = 2\rho A v_i^2 \tag{1}$$

Where,

T_h is the thrust from disk when rotor is in hover

ρ is the air density

A is the area of the disk

978-1-5386-3742-5/17/$31.00 © 2017 IEEE

v_i is the induced air velocity

Blade element theory is very useful when analyzes the airfoil and rotor performance. Blade element theory is applied to the blade in order to obtain the better rotor aerodynamics [11] since the momentum conservation theory does not consider the blade profile. First, a small cross-section, dy, of a propeller's one blade is considered at y meter when the blade is rotated clockwise at constant angular velocity Ω rad/sec as shown in Fig 1.

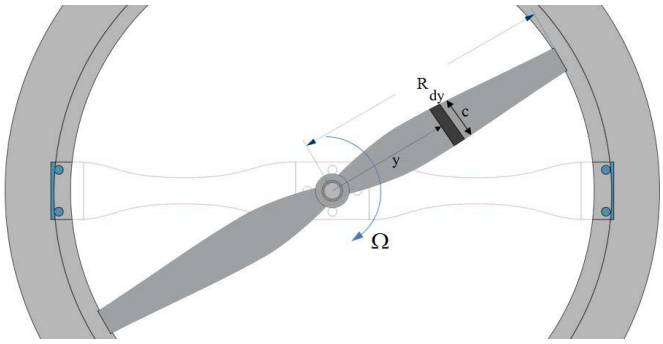

Fig. 1. Top view of the blade

The free body diagram of the section blade is shown in Fig 2. The blade is rotated at constant angular velocity and it creates the relative wind in the opposit direction. Air is now outflow from the bottom of the blade and creates the down force and also drags force.

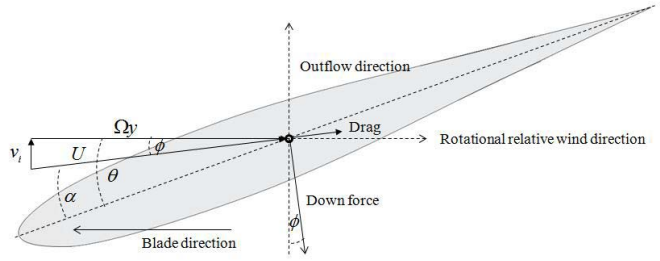

Fig. 2. Blade small cross section

Therefore, the down force of the cross section and the drag force are equal to (2) and (3) respectively.

$$dD_F = \frac{1}{2}\rho U^2 c C_L dy \tag{2}$$

$$dD = \frac{1}{2}\rho U^2 c C_d dy \tag{3}$$

Where,

D_F is the down force of blade section

U is the velocity of the wing through the air

c is the chord width

C_L, C_d is the lift coefficient and drag coefficient respectively

The down force coefficient is equal to the lift coefficient of the blade because it is a non-dimensionalised value and is depended on blade profile, Reynolds Number (RE) and angle of attack, α. Thrust of the section blade can be calculated by using (4) according to Fig 2.

$$dT = dD_F \cos(\phi) - dD \sin(\phi) \tag{4}$$

Where,

$\phi = \theta - \alpha$ is the effective angle of attack

Reynolds Number is an important dimensionless quantity in fluid mechanics that used to predict flow patterns in different fluid flow conditions. Reynolds number is the ratio between inertial forces and viscous forces which is relative to an internal movement of fluid due to different velocities. RE indicates the aerodynamic conditions of the considered blade operation condition and it can be calculated by equal (5).

$$RE = \frac{\rho v_i c}{\mu} \tag{5}$$

Where,

μ is the dynamic viscosity of the air

Blade profile is designed in such a way that it generates high lift force but low drag force, thus, the effective angle of attack is small and the angle of attack can be estimated as the angle of blade. Therefore, the thrust of the blade cross section and velocity of the wing through the air can be estimated as (6) and (7) respectively.

$$dT \cong dD_F \tag{6}$$

$$U \cong \Omega y \tag{7}$$

Then, the thrust coefficient of the cross section equals to (8)

$$dC_T = \frac{dT}{\rho A(\Omega R)^2} \tag{8}$$

Where,

R is the rotor radius

Substitute equation (2) to (8) and multiply by number of blade in the rotor, N, then, equation (8) becomes (9)

$$dC_T = \frac{1}{2}\frac{N\rho U^2 c C_L dy}{\rho A(\Omega R)^2} \tag{9}$$

Let define the solidity factor for constant chord blade as (10). The solidity factor is the ratio between the blade area and the rotating disk area.

$$\sigma = \frac{NcR}{\pi R^2} = \frac{Nc}{\pi R} \tag{10}$$

The total thrust efficient of the rotor is equal to total integration of all blade section and equation (9) becomes (11).

$$C_T = \frac{1}{2}\int_0^R \frac{N\rho U^2 c C_L}{\rho A(\Omega R)^2} dy = \frac{\sigma}{2}\int_0^1 C_L r^2 dr \tag{11}$$

Where, $r = y/R$

Regularly, the value of lift coefficient is vary along the blade and depends on RE. Therefore, the estimation of total thrust coefficient can be obtained by using the constant mean lift coefficient ($\bar{C}_L$) of the blade at y = 75% of the blade length and there is no twist in the blade, then, the estimated thrust coefficient becomes (12).

$$C_T = \frac{\sigma}{2}\int_0^1 \bar{C}_L r^2 dr = \frac{\sigma}{6}\bar{C}_L \tag{12}$$

The value of the mean lift coefficient can be obtained from the experiment in a wind tunnel or computed from the airfoil simulation software such as X-foil program [12] when assign the proper parameters. Finally, thrust force or down force of the one rotor system can be obtained as (13)

$$TR = \frac{1}{6}\sigma\rho A(\Omega R)^2 \bar{C}_L \tag{13}$$

Where,

TR is the total thrust that generated from one rotor set

B. *Double-Propellers Robot*

Robot consists of two rotor systems and four free wheels. Rotor system consists of one propeller driven by one actuating motor. The angle of the each rotor is independently adjustable by using servo motor. Two rotor systems are attached to the robot frame at the front and back of the robot chassis. Front rotor has a clockwise propeller while the back rotor has a counter-clockwise propeller, therefore, two rotors must rotate at different rotating directions in order to generate the down thrust force. Thanks to the different rotating direction from each rotor, the robot body will not rotate when robot is on to climbing surface if the surface's friction is large enough. The top view robot system is shown in Fig 3.

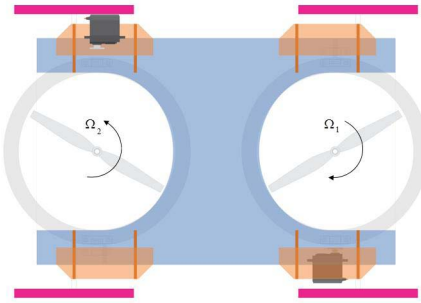

Fig. 3. Robot Diagram in the normalise plane to the climbing surface

In this research, the robot is considered when it is climbing a wall in vertical direction, therefore, for simplicity, robot can be considered as a planar robot. There are two possible conditions for the robot in order to climb the surface. First is when the robot has four contact points as shown in Fig 4. At this condition, four wheels are contacted to the climbing surface and the robot body is not fall out of the surface. Second condition happens when the robot has only two contacts point. In this condition, only two back wheels have contacts to the surface, thus, it is possible that robot will rotate and fall out of the climbing surface as shown in Fig 5.

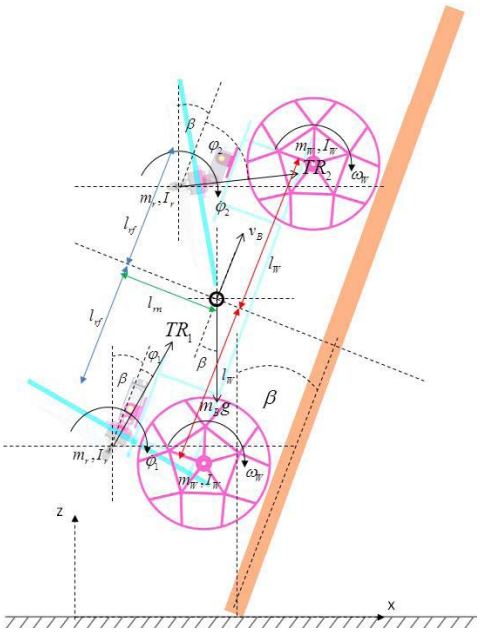

Fig. 4. Robot in the four contact points condition

Then the robot dynamics will be considered in two cases; four and two contact points. Dynamic of the robot is simple obtained by using conservation of energy of a planar wall-climbing robot. Lagrangian variable, L , is the difference between total kinetic energy, K , and total potential energy, P , of the robot and is expressed as $L = \sum K - \sum P$. Then, the Euler-Lagrange equation of motion is show in (14) when friction is neglected.

$$\frac{d}{dt}\left(\frac{\partial L}{\partial \dot{q}}\right) - \frac{\partial L}{\partial q} = \bar{f} \tag{14}$$

Where,

q is the states vector

$\bar{f}$ is the generalized force vector

When the robot is in the four contact points condition, robot body does not have rotation motion; robot body has only linear motion along x and y axes. Robot is always stick on the surface, thus, the states vector contains only four variables which are x , z , φ_1 and φ_2 . Therefore, by solving (14), the dynamics equation of the robot in the four contact points condition is equal to (15).

$$\begin{bmatrix} m_R & 0 & 0 & 0 \\ 0 & m_R & 0 & 0 \\ 0 & 0 & I_r & 0 \\ 0 & 0 & 0 & I_r \end{bmatrix} \begin{bmatrix} \ddot{x}_B \\ \ddot{z}_B \\ \ddot{\varphi}_1 \\ \ddot{\varphi}_2 \end{bmatrix} = \begin{bmatrix} TR_2 \sin(\beta+\varphi_2) + TR_1 \sin(\beta+\varphi_1) \\ TR_2 \cos(\beta+\varphi_2) + TR_1 \cos(\beta+\varphi_1) \\ \tau_{r1} \\ \tau_{r2} \end{bmatrix} \tag{15}$$

Where,

$m_R = 4m_W + 4I_W R_W^{-1} + m_B + 2m_r$

m_W, m_B, m_r are the wheel, body and rotor mass respectively

TR_1, TR_2 are the external thrust generated from rotor system.

τ_{r1}, τ_{r2} are the external torque applied to rotor system.

R_W is the wheel's radius.

I_W is an inertia of the wheel.

I_r is an inertia of the rotor system.

Equation (15) shows that the robot is simple to be controlled when four wheels are placed on the surface. External thrusts that applied to the robot are simple obtained by equation (13). But when the robot starts to fall out of the surface, the new state variable ψ is introduced to the system. Variable ψ is the angle of the robot measured to surface as shown in Fig. 5. In this research, the robot is operated for climbing a wall condition, thus, climbing the ceiling condition is not considered. Now, robot is in the two contact-points condition which only two back wheels have contacts to the surface while front wheels are freely in the air. In this condition, the value of ψ must be reduced in order to control the robot move back to the climbing surface and go back to four contact points condition. By solving (14), the dynamics equation of the robot in the two contact-points condition is equal to (16).

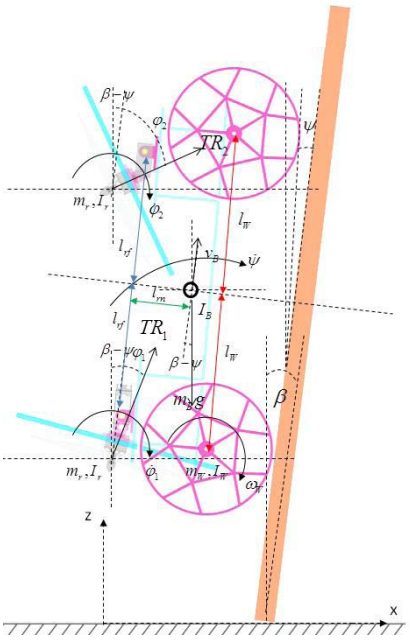

Fig. 5. Robot in the two contact points condition

$$\begin{bmatrix} m_R^* & 0 & 0 & 0 & 0 \\ 0 & m_R^* & 0 & 0 & 0 \\ 0 & 0 & \Delta & 0 & 0 \\ 0 & 0 & 0 & I_r & 0 \\ 0 & 0 & 0 & 0 & I_r \end{bmatrix} \begin{bmatrix} \ddot{x}_B \\ \ddot{z}_B \\ \ddot{\psi} \\ \ddot{\varphi}_1 \\ \ddot{\varphi}_2 \end{bmatrix} = \begin{bmatrix} f_x \\ f_z \\ -\tau_\psi \\ \tau_{r1} \\ \tau_{r2} \end{bmatrix} \quad (16)$$

Where,

$$m_R^* = 4m_W + 2I_W R_W^{-1} + m_B + 2m_r$$

$$\Delta = (8m_W + m_B + m_r)l_w^2 + m_r(2l_{rn}^2 + l_{rf}^2) + \frac{1}{2}I_B$$

$$f_x = TR_2 \sin(\beta - \psi + \varphi_2) + TR_1 \sin(\beta - \psi + \varphi_1)$$

$$f_z = TR_2 \cos(\beta - \psi + \varphi_2) + TR_1 \cos(\beta - \psi + \varphi_1)$$

$$\tau_\psi = f_x\sqrt{(l_w + l_{rf})^2 + l_{rn}^2} + f_z\sqrt{(l_w - l_{rf})^2 + l_{rn}^2} + \tau_{r1} + \tau_{r2}$$

l_W is the distant from center of robot to center of wheel

l_{rf} is the distant along robot's body direction from center of robot to center of rotor system.

l_{rn} is the distant from center of robot to center of rotor system in perpendicular direction to robot frame.

I_B is an inertia of the robot body.

From equation (15), value of ψ can be reduced by external thrusts and torques that applied to the robot system.

III. Real Robot

After robot mathematic model is obtained, the real robot is manufactured. Robot consists of four parts; robot body frame, wheels, rotor system and electronics system. Robot weight must be as small as possible. Therefore, robot wheels are made from the PLA thermal plastic. 3D printer is used to print the designed wheels. From the preliminary test, the rubber o-ring can be used as the robot tire. It has a good friction but it's heavy. Therefore, for this robot, the silicone sealant is used as the robot tire. Silicone sealant has a smaller friction coefficient than rubber but it generates enough friction for holding the robot to the surface. Moreover, silicone tire is much lighter than rubber tire. Finally, the wheel with Silicone tire is weight 47g. Robot wheel and Silicone tire are shown in Fig 6.

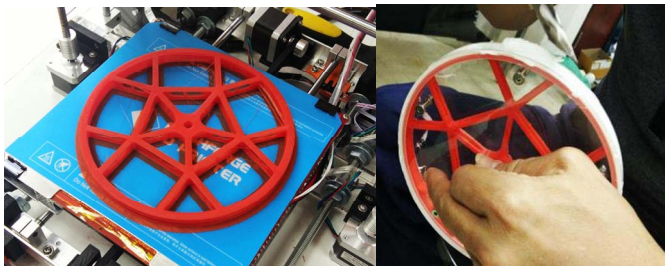

Fig. 6. Robot wheel(lift) and robot tire made from Silicone sealant(right)

Robot body frame is made from the polycarbonate because of its characteristic. Polycarbonate is a good material since it is light weight and strong. It is used in both robot body frame and the rotor systems. Polycarbonate sheet can be cut by using CNC machine. The cutting process and final product are shown in Fig 7. Rotor system consists of servo motor, brushless DC motor and propeller. 1200KV brushless DC motor is selected as the actuating motor that generates thrust. This motor is operated at 12V. APC propeller is selected for the robot since it is designed similar to the NACA 4412 airfoils characteristic. This blade has angle of attack around

10.24° .The propeller is attached to the brushless motor inside a polycarbonate protection ring. Angle of this rotor system can be changed by using servo motor. The completed rotor system is shown in Fig. 8. Since the selected propeller is similar to NACA 4412 airfoils, thus, by using X-foil software, the thrust coefficient can be obtained as shown in Fig. 9. when the propeller is operated at the ultra-small Reynolds number between 12000 to 18000.

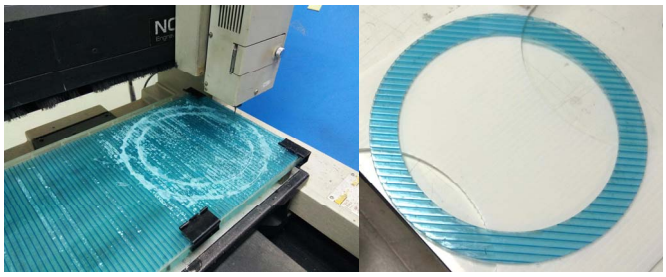

Fig. 7. CNC cutting the polycarbonate sheet(left) and product(right)

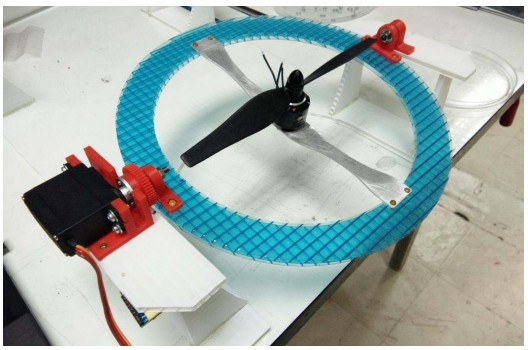

Fig. 8. Assembled rotor system

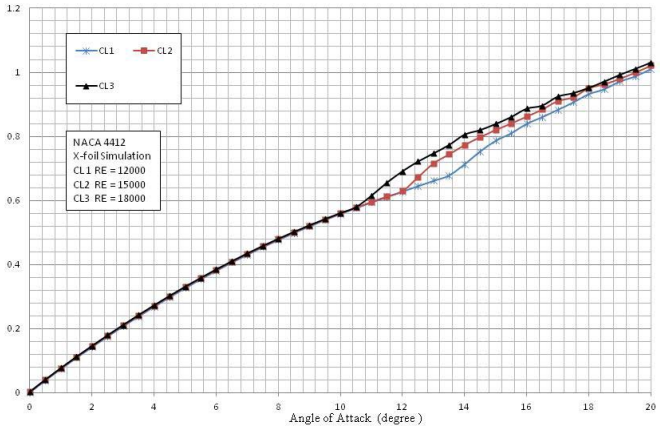

Fig. 9. CL of the selected propeller when RE =12000, 15000 and 18000

Then, rotor systems and robot body frame are assembled together by using connector made from PLA plastic. Nuts and bolts cannot be using in this robot because their weight. The rivet is used as a permanent mechanical fastener for fasten all robot part together. The assembled robot is shown in Fig. 10. The final part of the robot system is the electronics system. Arm-Cortex M3 is selected as robot low-level embedded controller. This controller is operated at 72 MHz. An Inertia Measurement Unit (IMU MPU6050) which is a combination of accelerometer and gyro sensor is used to construct the observer system in order to determine the robot angle and angular velocity. Two 60A BLDC ESC is used as a brushless motor driver which can drive each brushless motor up to 60A continuous driving current. Four cells Lithium-polymer battery is selected as robot power source. Two Hi-tech servo motor are used to change a rotor system angle. Eight channels radio receiver is integrated to the system in order to manually control the robot. The diagram of the electronics system is shown in Fig 11. Finally, the total weight of the robot is 1.35 kg.

Fig. 10. Assembled robot

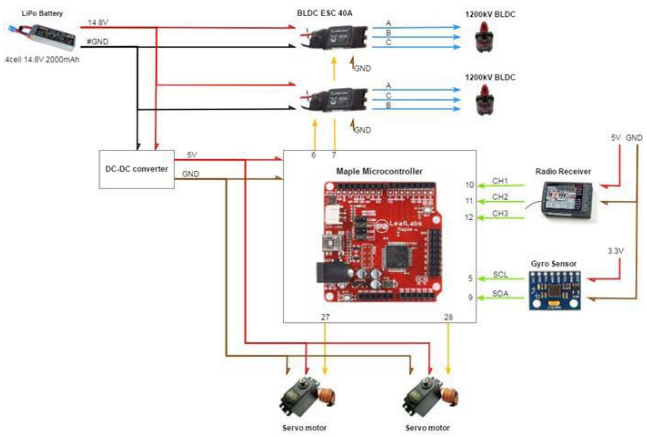

Fig. 11. Electronics system

After eletronics system is installed to the robot hardware then the robot control software is considered. FreeRTOS [13] is a RTOS that is designed to fit into a small calculation power and limited resources microcontroller such as an Arm-Cortex M3. FreeRTOS is implemented for this wall-climbing robot. Scheduler time slice has be set to 1 msec. There are 4 tasks which is a radio task, IMU task, brushless DC motor control task and servo motor control task as shown in Fig. 12. Radio task is a event based task that will run whenever command signal is captured by the radio receiver. This task is used retrive command for a manual operation. IMU task is a periodic task that executed every 10 msec. This task acquires,

fuses data from IMU sensor via I2C protocol and calculates and combines necessary control signal and command signal which be sent to brushless and servo tasks. Brushless and servo tasks are also periodic task that executed every 10 msec. Brushless and servo task get motor's speed command and rotor command angle from IMU task via global variables respectively.

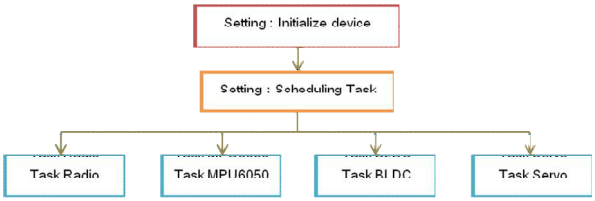

Fig. 12. Robot Tasks

IV. Experiments

In this topic, the robot experiments are conducted. First, the rotor system is experimented in order to obtain the real output thrust force information. The output thrust force is experimented by applying throttle command to the brushless motor via BLDC ESC motor driver. The output thrust force is measured from the weighing machine. Experiment is shown in Fig 13. and the result is shown in Fig 14.

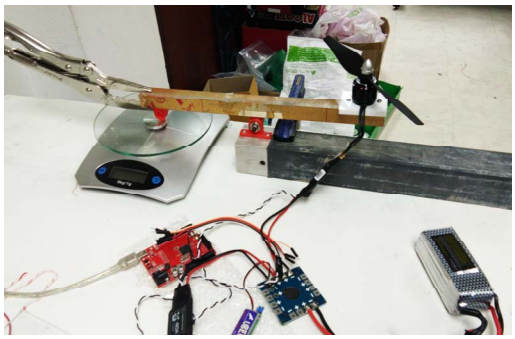

Fig. 13. Thrust force testing

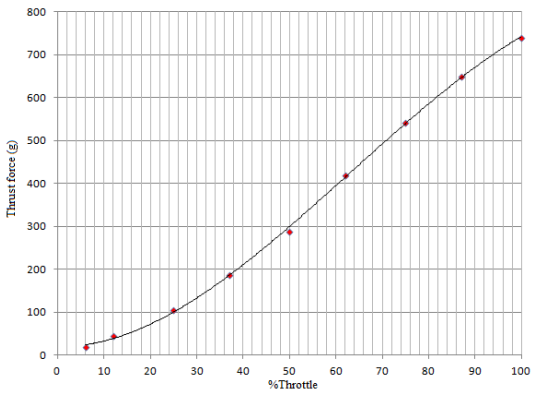

Fig. 14. Relationship between %throttle and output thrust force of a rotor.

The result shows that relationship between applied %throttle and the output thrust is estimated linear. The result also confirms that the propeller has similar characteristic as NACA 4412 and the thrust force is close to value that calculated from equation (12) when the coefficient is simulated from X-foil at the designed operating RE number. By analysing static condition of the robot when climbing the wall, if the output thrust force is set to 70% of full throttle, it is sufficient for the robot in order to hold itself to the wooden surface up to 85 degrees. The maximum climbing angle is confirmed by experiments as shown in Fig. 15. In this experiment, the %throttle is set to 70% and φ_1 and φ_2 is set to zero to generate smallest thrust force in the x direction. The climbing angle is increased continuously until robot starts to falling-out of the surface.

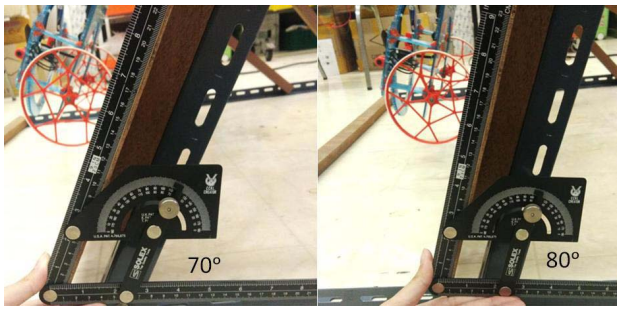

Fig. 15. The maximum climbing angle experiments

Then, 90 degrees wall-climbing experiment is conducted. The robot is attached to the protection sling in order to protect the robot hardware when it is unstable and fall-out of the surface. The setup is shown in Fig. 16. and the experiment result is shown in Fig. 17.

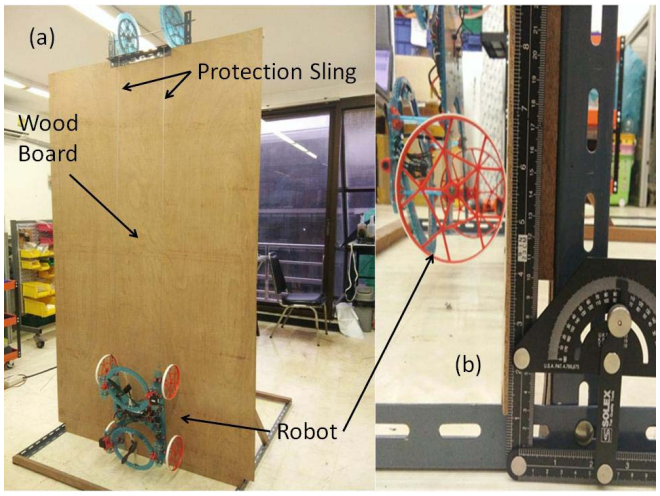

Fig. 16. 90 degrees experiment setup

From the experiment shown in Fig. 17 and measured robot angle in Fig 18, at the beginning robot (1) is in the two contact points condition. Two back wheels are contact to the wooden surface while two front wheels are stationary in the air. The input external thrust force then push robot to the surface and changes from the two to four contact points condition (2). After that, robot can easily climb the wall (3) (4). Results show that the designed robot can be controlled By using the

actuating thrust and change of rotor system angle, the robot can climb the desired surface and have ability to move itself back to the surface when the robot starts to fall out of the wall.

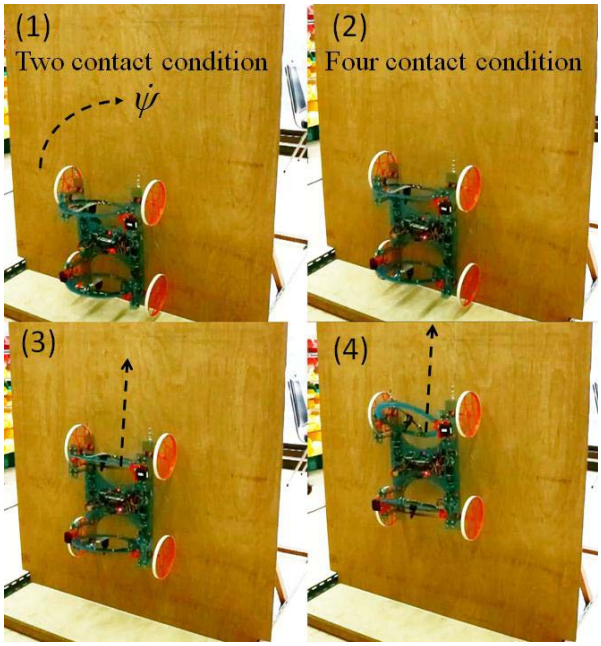

Fig. 17. Robot climbing a wooden wall

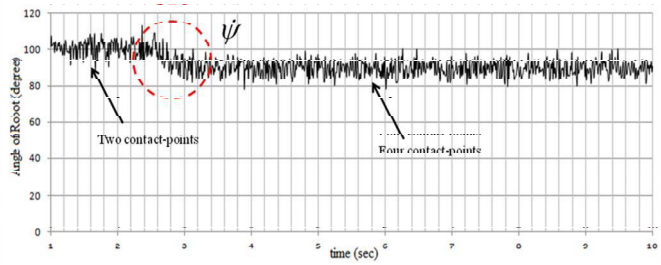

Fig. 18. Angle of Robot measured from IMU

V. Conclusion and Future Work

Propeller type wall-climbing robot is introduced in this research. Aerodynamics of the propeller blade is found by using the momentum conservation and blade element theories. Then, thrust force that generated from one rotor system is found. Robot dynamics is simple obtained by solving Euler-Lagrange equation of motion on two robot conditions. Two contact-points condition is happen when only two robot back wheels are attached to the climbing surface while other wheels is free in the air. This condition happens when robot starts to fall-out of the surface. Luckily, it is possible to drive robot back to the surface by using actuating thrust from propellers and change of rotor system angle. The four contact-points condition is the normal operation condition for the wall-climbing robot when all wheels are stick to the climbing surface. After robot mathematic model is found, the real robot is manufactured. Robot wheels are made from PLA plastic using 3D printer. Unlike the regular tires, robot tires are made from the silicone sealant in order to reduce robot weight. Polycarbonate sheet is used for robot body frame and rotor system. Brushless DC motor combined with NACA 4412 propeller is used in rotor system to generate external thrust. Angle of each rotor system can be controlled by servo motor. Robot electronics system consists of Arm-Cortex M3 microcontroller, motor driver, radio receiver and IMU. FreeRTOS is implemented to the controller in order to handle several tasks simultaneously. Then, robot performance is tested in experiments. Robot can climb the wooden wall with 90° inclination. Experiment also shows that the robot has ability to drive itself back from the falling down situation to the regular operation condition.

In the next research, the control algorithms are focused and explained. Robot dynamics will be further explored. The robot will be experimented in the real-life environments such as in the building wall, factory chimney and especially in the oil and gas industries. The final version of the designed robot will have ability to fly and climb wall and ceiling and it will be the hybrid robot between Quadrotors and propellers type wall-climbing robot.

References

[1] J. Grieco, M. Prieto, M. Armada, and P. Santo, “A six-legged climbing robot for high payloads,” Proceedings of the 1998 IEEE International Conference on Control Applications, pp. 446-450, Trieste, Italy, 1998.

[2] W. Shen, J. Gu and Y. Shen, “Proposed Wall Climbing Robot with Permanent Magnetic Tracks for Inspecting Oil Tanks,” Proceedings of the IEEE International Conference on Mechatronics & Automation, Niagara Falls, Canada, July 2005, pp. 2072 - 2077.

[3] M. O. Faruq Howlader and T. P. Sattar, "Development of magnetic adhesion based climbing robot for non-destructive testing," 2015 7th Computer Science and Electronic Engineering Conference (CEEC), Colchester, 2015, pp. 105-110.

[4] A. Nishi, “A wall climbing robot using propulsive force of propeller.,” Fifth International Conference on Advanced Robotics 'Robots in Unstructured Environments, vol.1, 1991, pp. 320-325.

[5] P. Beardsley, “VertiGo – A Wall-Climbing Robot including Ground-Wall Transition,” Disney Research Zurich, 2015.

[6] S. Panich, “Development of a Wall Climbing Robot,” Journal of Computer Science, 2010, pp. 1185-1188.

[7] M. Wagner, X. Chen, M. Nayyerloo, W. Wang and J. G. Chase, "A Novel Wall Climbing Robot Based on Bernoulli Effect," 2008 IEEE/ASME International Conference on Mechtronic and Embedded Systems and Applications, Beijing, 2008, pp. 210-215.

[8] C. Menon, M. Murphy and M. Sitti, “Gecko inspired surface climbing robots,” IEEE International Conference on Robotics and Biomimetics, 2004, ROBIO 2004. Pp. 413-436

[9] S. Kim, M. Spenko, S. Trujillo, B. Heyneman, D. Santos and M. R. Cutkosky, “Smooth Vertical Surface Climbing With Directional Adhesion,” IEEE Transactions on Robotics, vol. 24, no. 1, Feb. 2008 , pp. 65-74

[10] J. Seddon, Basic Helicopter Aerodynamics, 1st ed., Oxford: Blackwell Science, Osney Meas, 1990, pp. 5-6.

[11] D. Honnery, Introduction to the Theory of Flight, Gracie Press, Northcote, Victoria, 2000, pp. 94, pp. 112.

[12] M. Drela, X-Foil Subsonic Airfoil Development System, http://raphael.mit.edu/xfoil/, August 2004.

[13] http://www.freertos.org